RSC Advances

ROYAL SOCIETY OF CHEMISTRY

PAPER

View Article Online
View Journal | View Issue

Check for updates

Cite this: *RSC Adv.*, 2025, **15**, 24668

Hydrogen adsorption and dissociation on Au_nY ($n = 1$–12) nanoclusters: a DFT investigation†

Nguyen Van Dang,[a] Ngo Thi Lan,*[a] Nguyen Thi Mai,[b] Son Tung Ngo,[cd] Phung Thi Thu[e] and Nguyen Thanh Tung[b]

Received 17th March 2025
Accepted 4th July 2025

DOI: 10.1039/d5ra01901j

rsc.li/rsc-advances

The interaction between nanomaterial systems and hydrogen has recently emerged as a compelling study model, offering valuable insights for designing materials with applications in nanotechnology, catalysis, and energy storage. Among these, transition metal-doped gold clusters exhibits intriguing stability and electronic properties, making them promising candidates for hydrogen related processes. In this study, we employ density functional theory (DFT) to investigate the interaction between H_2 molecules and small-sized gold clusters doped with yttrium. Our finding reveals that most of the bare cluster structures remain intact during the H_2 adsorption, regardless of whether the process occurs molecularly or dissociatively. A comprehensive analysis indicates that the preferred adsorption configuration is governed by multiple factors, including adsorption site (surface *vs.* encapsulated), relative electronegativity, and the atomic coordination number. The calculations demonstrate that dissociative adsorption of H_2 on Au_6Y and $Au_{11}Y$ clusters is both thermodynamically and kinetically favorable. However, for Au_nY ($n = 1$, 4–5, 8, 10) dissociative adsorption is hindered by a significant energy barrier before reaching the final state, while for species with $n = 2$, 3, 7, and 9 molecular adsorption is more favorable due to intrinsic energy preferences. This study provides fundamental insights into the adsorption sites and detailed analysis of adsorption kinetics on Au_nY clusters, laying the groundwork for further theoretical an ed experimental investigations into the hydrogenation process in nanostructured materials.

1. Introduction

Nowadays, hydrogen has been envisioned as a key energy carrier for sustainable development of the future economy, meeting essential environmental and energy requirements.[1–3] Compared to traditional fuels like gasoline (44 MJ kg^{-1}) and diesel (45.6 MJ kg^{-1}),[4,5] hydrogen offers the highest energy density per unit mass (~120 MJ kg^{-1}) and conversion efficiency and can be produced through water-splitting reactions without CO_2 emissions. Moreover, it can be conveniently stored in various forms, including gaseous, liquid, or metal hydrides.[6–8] However, the practical implementation of hydrogen energy storage after generation and during transport faces significant challenges, primarily due to its kinetic stability under ambient conditions and the low energy density per unit volume of solid storage materials.

To address this bottleneck, various strategies have been explored.[9–12] Among them, metal hydride materials have garnered special attention as model solid-state hydrogen storage systems, offering a more compact and secure alternative. They provide the possibility of preventing critical operating conditions like high pressures and elevated temperatures, which are typical of conventional compressed gas and liquefied hydrogen storage.[13] To enhance the practical prospect of metal hydride, a deeper understanding of the interaction between hydrogen and potential surface at the molecule level is essential. Therefore, nanoclusters consisting of a few atoms have emerged as promising candidates for providing fundamental insights into potentially reactive sites, given significant variation in physical and chemical properties with size and composition.

Among various metal nanoclusters, gold nanoclusters (Au_n) are considered particularly advantageous due to their superior stability, abundance, and cost-effectiveness, even surpassing palladium and platinum in many aspects. While gold is chemically inert in its bulk form, it exhibits remarkable catalytic activity at the nano scale. For example, gold nanoclusters have shown promising performance in catalytic processes such as water-splitting reaction[14] and CO oxidation.[15] Interestingly, this

---

[a] *Institute of Science and Technology, TNU-University of Sciences, Tan Thinh Ward, Thai Nguyen City, Vietnam. E-mail: lannt@tnus.edu.vn*

[b] *Institute of Materials Science, Vietnam Academy of Science and Technology, Hanoi, Vietnam*

[c] *Laboratory of Biophysics, Institute for Advanced Study in Technology, Ton Duc Thang University, Ho Chi Minh City, Vietnam*

[d] *Faculty of Pharmacy, Ton Duc Thang University, Ho Chi Minh City, Vietnam*

[e] *University of Science and Technology of Hanoi, Vietnam Academy of Science and Technology, 18 Hoang Quoc Viet, Hanoi, Vietnam*

† Electronic supplementary information (ESI) available. See DOI: **https://doi.org/10.1039/d5ra01901j**

catalytic behavior is highly dependent on their geometric structure. Bootharaju and co-workers[16] investigated the $Au_{12}Ag_{32}/TiO_2$, system, which features a gold icosahedral core encapsulated by a silver dodecahedral shell. Their finding revealed a substantial enhancement in solar H_2 production efficiency, approximately 6.2 and 37.8 times higher than those of Ag_{44}/TiO_2 and bare TiO_2, respectively. Furthermore, key factors influencing the reactivity and catalytic potential of gold nanoclusters include cluster size, atomic composition, and charge state.[17–19] By tailoring these parameters, such as through doping or precise control of cluster size, researchers can design tunable materials optimized for specific catalytic processes. For instance, both experimental and theoretical studies have explored O_2 activation on small-sized anionic Au_n^- clusters.[20] S. Pal and D. Manzoor have compared the catalytic efficiency of Au_8, Pd_8, $Au_{8-n}Pd_n$ ($n = 1$–7), Au_7Si,[21,22] Au_{18} and endohedral $Au_{18}M$ (M = Na, K, Mg, Ca, Al, Ga) cages,[23] and Al-, Hf-, and Ge-doped Au_{20} cages.[24] Similarly, Zeng and co-workers[25] using DFT calculation studied the catalytic behavior of sub-nanometer-sized gold nanoclusters supported on TiO_2. They observed that cluster shape and size significantly influenced catalytic performance, with adsorption energies for O_2 and CO decreasing as the cluster size increased within the range of 16–35 atoms.[15] Recent studies have also highlighted the emerging role of hydrogen atoms as dopants in gold nanoclusters.[26] Beyond their electronegativity, hydrogen atoms can induce chemisorption and activation on previously inert or closed-shell gold clusters,[27] modulated by cluster shape,[28,29] and charge state.[30] This, in turn, enhances the adsorption and activation of O_2 and CO molecules, opening new directions for designing advanced gold-based catalysts.

Research efforts have expanded beyond the studies of O_2 adsorption and CO oxidation to include investigations of metal nanoclusters and their alloys in order to deepen our understanding of the kinetics and dynamics of hydrogenation reactions. Numerous density functional theory (DFT)[31–34] studies have investigated the adsorption and dissociation of hydrogen on metal nanoclusters. The H_2 absorption process has been found to strongly depend on the physical and chemical properties, structural, size, and composition of nanoclusters, as demonstrated in 3d transition metal (Sc–Zn)-doped Cu clusters[35] and $Au_{24}M$, $Au_{36}M$ (M = Pt and Pd).[36] Theoretical studies have demonstrated that the incorporation of a Pt dopant can significantly alter the electronic structure of gold nanoclusters Au_{n+1} ($n = 1$–12), thereby enhancing their reactivity toward H_2 molecules.[37] Li and coworkers investigated the effect of adsorbed hydrogen atoms on the geometric and electronic structures of alkali-doped gold nanoclusters, providing insights into hydrogen-cluster interaction.[38] Additionally, the adsorption and dissociation behavior of $TiMg_n$ ($n = 1$–12) clusters has been examined DFT, revealing key factors that govern their hydrogen activity.[39] Furthermore, mass spectrometry and infrared multiple photon dissociation spectroscopy combined with theoretical calculations, have provided insights into the competition between molecular and dissociative hydrogen chemisorption, which is highly dependent on the size of cationic aluminum-doped Rh clusters.[40,41] Recently, Lan *et al.* conducted comparative studies on the influence of 3d transition metal atoms on hydrogen adsorption and dissociation by examining size-dependent Ag_nCr ($n = 2$–12) clusters and composition-dependent Au_9M^{2+} (M = Sc–Ni) clusters.[42,43] Their research has revealed that Ag_3Cr, Ag_6Cr, and Au_9Ti^{2+}, clusters exhibit the ability to adsorb and dissociate H_2, leading to the formation of metal hydrides even at room temperature.

Additionally, 4d transition metal atoms have shown significant potential for hydrogen storage, attributed to their enhanced stability, fully filled electron configurations across multiple energy levels, diverse oxidation states, and distinct chemical properties compared to their 3d counterparts.[44,45] Moreover, the lower electronegativity of 4d transition metals relative to 3d elements influences their interaction with hydrogen, raising several intriguing questions, such as how charge transfer occurs in clusters and the nature of interactions between dopant clusters and hydrogen molecules. To address these questions, the effects of boron and 4d transition metal (Y–Mo) on hydrogen adsorption and storage properties have been systematically investigated.[45–47] Notably, the impact of charge transfer, electronegativity, and the atomic radius of the dopant elements on the catalytic mechanism and hydrogen storage capacity of MgH_2 clusters has been clarified.[48,49] C.S. Sergio *et al.* have clarified the correlation between hydrogen storage capacity and the surface binding energy of 4d transition metal-doped carbon nanoflakes.[50] Recent work by J. Barabás *et al.*, combining gas-phase reaction investigations and DFT computations, has demonstrated that the catalytic activity of gold cation clusters (Au_n^+) and yttrium-doped gold ($Au_{n-1}Y^+$, $n = 4$–20) clusters can be effectively tuned by cluster size, charge state, and dopant introduction.[51] While initial studies have explored the influence of 4d transition metals on cluster stability and reactivity, a systematic investigation of the hydrogen storage mechanism in noble metal clusters doped with 4d transition metals remains lacking. A deeper understanding of the kinetics and dynamics of hydrogenation reactions in precious metal species and their alloys could pave the way for new research directions in hydrogen storage materials.[52,53]

Driven by the pursuit of nanocluster materials for efficient hydrogen storage, this study aims to theoretically explore the critical role of yttrium doping in H_2 adsorption and dissociation on small gold clusters. Using DFT calculations,[54] we systematically analyze the geometrical, relative stability, bonding characteristics, electronic properties, and adsorption energies of Au_nY ($n = 1$–12) clusters. The insights gained from this study provide a deeper understanding of the influence of 4d transition metal dopants on hydrogen adsorption and dissociation mechanisms. Furthermore, these findings offer valuable guidelines for future experimental studies, aiding the rational design of advanced nanomaterials for hydrogen storage applications.

2. Computational method

This work uses the DFT calculations implemented in the Gaussian 09 program[55,56] in combination with GaussView, to predict the geometric and electronic structures of Au_nY ($n = 1$–

12) clusters in their ground state, along with their molecularly and dissociatively adsorbed variants $Au_nY–H_2$ and $Au_nY–2H$. To generate initial cluster structures, two complementary approaches were employed: (1) a stochastic algorithm was used to explore a broad range of feasible Au_nY ($n = 1–12$) configurations;[57] (2) manual structure construction, in which a Y atom systematically replaced an Au atom at all possible positions within the cluster. Subsequently, hydrogen adsorption configurations were investigated based on the lowest-energy Au_nY ($n = 1–12$) structures, where a single H_2 molecule or two dissociated H atoms were attached at various adsorption sites.

Computationally, predicted structures were first optimized by the TPSSTPSS functionals in combination with the cc-pVDZ-pp basis set for Au and Y atoms, and LanL2DZ for H atoms. For each cluster size, various structural and spin configurations were explored and subjected to the convergence criteria. Nevertheless, only species with relative energies less than 2.0 eV were selected for single-point energy recalculations at the same functional level but with an enhanced basis set, specifically cc-pVTZ-pp for Au and Y atoms and LanL2DZ for H atoms. This approach represents a balanced trade-off between computational accuracy and efficiency and has been shown to be reliable for 4d transition metal-doped noble metal systems.[58] To validate the accuracy and reliability of our computational methodology, we compared binding energies (BE, eV) of Au_2, AuY, AuH, and YH dimers across different functionals, including TPSSTPSS, BP86, BPW91, BLYP, and PBEPBE. Tables 1 and S1† summarize the results and benchmarks them against available experimental data, confirming that the TPSSTPSS/cc-pVTZ-pp (for Au and Y) and LanL2DZ (for H) combination yields the closest agreement with experimental values. The self-consistent field (SCF)[59] calculations were conducted with a convergence threshold of 2.0×10^{-5} Hartree per Å for gradients and 5.0×10^{-3} Å for displacements. The stability of the lowest-energy structures was further confirmed by calculating harmonic vibrational frequencies, ensuring they correspond to true minima on the potential energy surface. To reinforce the robustness of the ground-state optimization, multiple spin multiplicities were examined for each structure. The electronic configurations of all lowest-energy structures were analyzed using the natural bond orbital (NBO) method.[60] To explore the reaction mechanisms, transition-state (TS) geometries were identified using the quadratic synchronous transit (QST) method,[61,62] with relaxed potential energy surface (PES) scans along appropriate internal coordinates. To further verify the transition states, intrinsic reaction coordinate (IRC) calculations were performed, ensuring a continuous and valid connection between reactants and products.

3. Optimized geometrical structures

We first optimized the lowest-energy structures of bare Au_nY clusters and then examined both molecular and dissociative adsorption of hydrogen, leading to the formation of $Au_nY–H_2$ and $Au_nY–2H$ clusters, respectively. To ensure the stability of the obtained geometries, we conducted frequency calculations, confirming the absence of imaginary frequencies in all optimized structures. While multiple geometrical and spin isomers exist for each stoichiometry, only the lowest-energy structures of Au_nY, $Au_nY–H_2$, and $Au_nY–2H$ clusters were selected for further discussion of hydrogen adsorption behavior, as shown in Fig. 1. Other low-lying isomers for $Au_nY–H_2$ and $Au_nY–2H$ clusters are provided in the ESI.†[46]

Our results indicate that the stable spin configurations of Au_nY ($n = 1–12$) clusters follow an alternating pattern with a singlet spin state for odd n and a doublet for even n. The lowest-energy Au_nY structures tend to adopt a cage-like form as the cluster size increases, where the Y atom prefers a highly coordinated position. Interestingly, the structural framework of Au_nY ($n = 1–12$) clusters undergoes significant reconstruction upon yttrium doping, deviating from the planar configuration of pure Au_n clusters ($n \leq 11$).[64] Unlike pure gold clusters, where the first 3D structure appears at $n = 12$, the introduction of a Y atom stabilizes 3D geometries at much smaller sizes, starting from $n = 4$, where four Au atoms coordinate around the Y dopant. The lowest-lying isomers of Au_nY ($n = 5–8$) retain a 2D morphology, whereas larger clusters ($n = 9–12$) exhibit 3D structural preferences. These findings align well with theoretical predictions and far-infrared spectral studies of yttrium-doped gold clusters.[65]

Our calculations suggest that hydrogen adsorption does not significantly alter the geometric structure of bare Au_nY clusters, except for Au_5Y, where H_2 preferentially attaches to energetically unstable bridge sites (Au–Y and Au–Au). Similar behavior has been observed in transition metal-doped clusters.[41–43,66] For Au_nY ($n = 1–5$, 7, 9, and 12), the hydrogen molecule favors direct attachment to the Y dopant, attributed to differences in electronegativity χ between Y (1.22), H (2.2), and Au (2.54). Fundamentally, hydrogen bonding arises from electrostatic attraction, facilitated by charge transfer between atoms with significant electronegativity differences. Consequently, bonds between the low-electronegativity Y atom and high-electronegativity H atom are more favorable, in agreement with previous reports, where surface impurities are among the most favored adsorption sites for a hydrogen molecule on transition metal doped clusters.[41–43,67] Furthermore, hydrogen adsorption is not solely governed by electronegativity differences but also strongly influenced by atomic coordination number (N). Lower

Table 1 Calculated binding energies (BE, eV) for AuH and YH dimers using various functionals in combination with cc-pVTZ-pp for Au and Y atoms, and LanL2DZ/SDD for H atoms

	BP86		PW91		BLYP		PBEPBE		TPSSTPSS		
Dimer	LanL2DZ	SDD	LanL2DZ	SDD	LanL2DZ	SDD	LanL2DZ	SDD	LanL2DZ	SDD	Experiment[63]
AuH	3.07	3.11	3.02	3.00	2.94	2.97	2.94	2.98	3.00	3.02	3.03 ± 0.08
YH	2.90	3.12	2.74	2.82	2.88	3.02	2.79	2.85	2.94	3.23	—

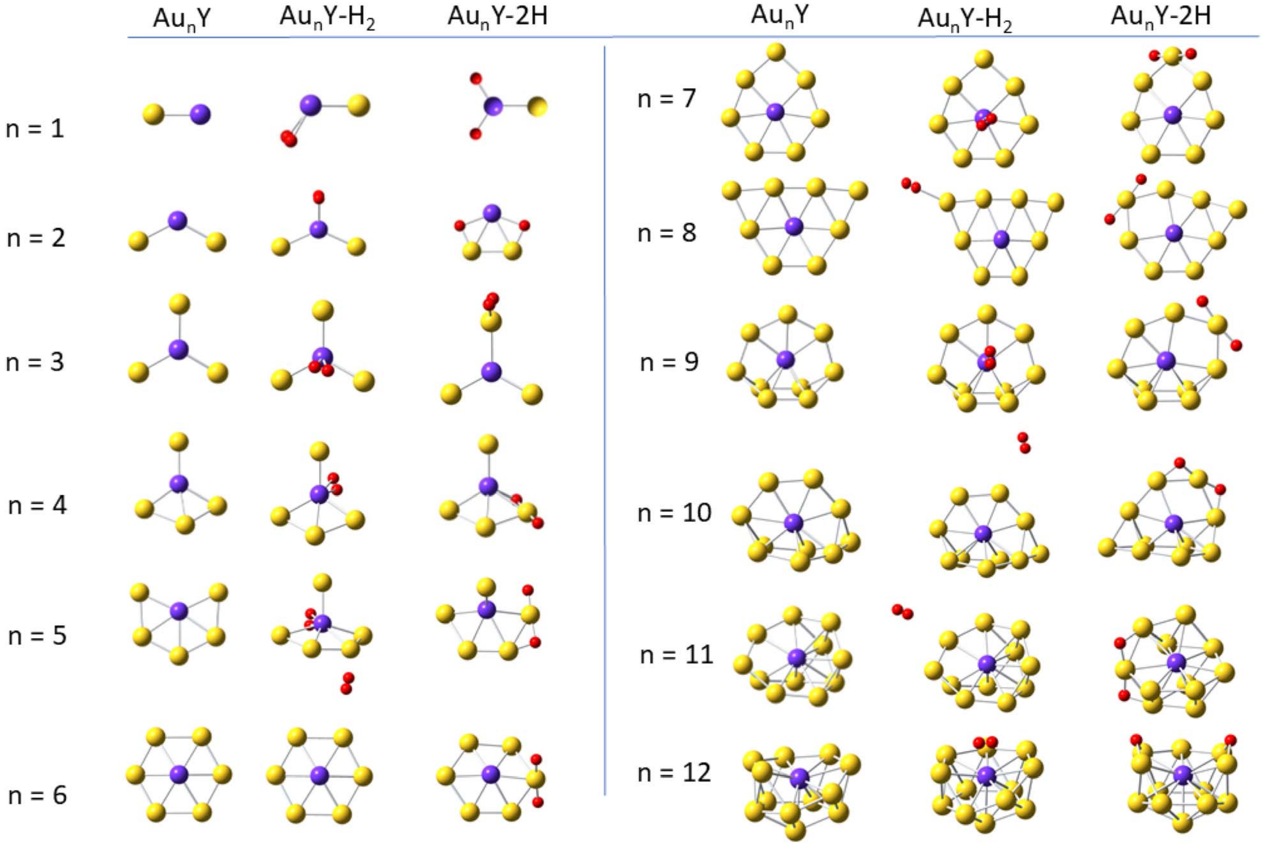

Fig. 1 Optimized structures of Au$_n$Y, Au$_n$Y–H$_2$, and Au$_n$Y–2H clusters ($n = 1$–12). The yellow, purple, and red spheres represent Au, Y, and H atoms, respectively.

coordination numbers correspond to higher surface activity, facilitating stronger H$_2$ adsorption.[68] Consequently, atomic clusters with low-coordination sites exhibit enhanced hydrogen interaction capability. For example, experimental and theoretical studies on singly rhodium-doped cationic aluminum clusters (Al$_n$Rh$^+$) using time-of-flight mass spectrometry and infrared multiple photon dissociation, in combination with DFT calculations, have demonstrated that hydrogen preferentially binds to the Al atom rather than the Rh impurity in cluster sizes where Rh is coordination-saturated or encapsulated.[41] This principle helps explain the behavior observed in Au$_6$Y–H$_2$, Au$_8$Y–H$_2$, Au$_{10}$Y–H$_2$, and Au$_{11}$Y–H$_2$ clusters, where a competition between electronegativity and coordination occurs as H$_2$ preferentially attaches to a low-coordination Au vertex ($N_{\mathrm{Au}} = 2$ or 3) instead of the highly coordinated Y impurity ($N_{\mathrm{Y}} = 6$, 8, or 9). A similar hydrogen adsorption trend has been reported for the clusters Al$_n$Cr, Ag$_n$Cr, Au$_9$M^{2+}, Al$_n$Rh^{2+}, and Mg$_n$Co, further reinforcing the critical role of coordination number in determining the preferred hydrogen adsorption site.[41–43,66,69]

Upon molecular adsorption, the hydrogen molecule may dissociate, triggering a structural transformation of the bare clusters.[70] However, the ground-state geometry of Au$_n$Y clusters generally remains intact upon hydrogen adsorption, with only minor distortions observed in Au$_2$Y–2H, Au$_5$Y–2H, and Au$_8$Y–2H. As illustrated in Fig. 1, following H$_2$ dissociation one Au atom shifts closer to another Au atom in Au$_2$Y–2H, while in Au$_5$Y–2H and Au$_8$Y–2H, a single Au atom is slightly displaced from two-membered and three-membered Au chains, respectively. Notably, both cluster size and the position of the Y dopant significantly influence H$_2$ dissociation and adsorption behavior, which can be categorized into two distinct trends. For small clusters ($n = 2$–4), individual hydrogen atoms preferentially bind to the surface Y atom, typically at the Au–Y bridge site. As the cluster size increases ($n = 5$–12), the Y atom becomes progressively encapsulated by surrounding Au atoms, leading to H atoms favoring Au–Au bridge adsorption rather than direct interaction with Y. This trend is in good agreement with previous investigations.[43] In the case of AuY–2H, both H atoms preferentially adsorb on top of the Y surface site, highlighting the role of dopant coordination and atomic arrangement in governing hydrogen interaction dynamics.

4. Relative stability

The relative stability of a clusters is a key parameter that provides insight into its bonding or dissociation energy, which are critical in determining reactivity and stability in chemical reactions. This stability is typically assessed through average binding energies (BE, in eV) calculations. The BE is defined as the mean energy difference between the sum of the total energies of all isolated constituent atoms and the total energy of the cluster. The calculation follows the equations below:

$$\mathrm{BE}(\mathrm{Au}_n\mathrm{Y}) = \frac{1}{n+1}[nE(\mathrm{Au}) + E(\mathrm{Y}) - E(\mathrm{Au}_n\mathrm{Y})] \tag{1}$$

$$\mathrm{BE}(\mathrm{Au}_n\mathrm{Y}-\mathrm{H}_2) = \frac{1}{n+3}[nE(\mathrm{Au}) + E(\mathrm{Y}) + 2E(\mathrm{H}) - E(\mathrm{Au}_n\mathrm{Y}-\mathrm{H}_2)] \tag{2}$$

$$\mathrm{BE}(\mathrm{Au}_n\mathrm{Y}-2\mathrm{H}) = \frac{1}{n+3}\left[nE(\mathrm{Au})_{E(\mathrm{Y})} + 2E(\mathrm{H}) - E(\mathrm{Au}_n\mathrm{Y}-2\mathrm{H})\right] \tag{3}$$

Here, E represents the total energy of the clusters or individual atoms. The binding energy (BE) values of Au_nY (n = 1–12) clusters range from 1.59 to 2.58 eV, as shown in Fig. 2 and Table 2. A notable increase in BE is observed for bare Au_nY clusters in the small-size range (n = 1–3), rising sharply from 1.59 eV to a peak of 2.55 eV. This trend persists in the presence of molecular hydrogen adsorption, although the increase in BE (from 1.96 eV to 2.48 eV) remains less pronounced compared to bare clusters of the same size. In contrast, for dissociative adsorption (Au_nY–2H), BE values gradually decrease from 2.38 eV to 2.08 eV. In contrast, the BE for dissociative adsorption Au_nY–2H exhibit a rough decrease from 2.38 to 2.08 eV. More remarkably, for larger clusters (n = 4–12), the BE values remain relatively stable, suggesting that these clusters exhibit greater stability after hydrogen release compared to smaller clusters (n = 1–3). Furthermore, the higher BE values of Au_nY–2H clusters (for n = 4–6, 8, 10 and 11) compared to their molecularly adsorbed Au_nY–H counterparts indicate that H_2 dissociation following molecular adsorption is more favorable at these sizes. This finding aligns well with the high intrinsic stability of bare Au_6Y clusters.[65] In contrast, for clusters with n = 1–3, 7, and 12, dissociative adsorption is energetically unfavorable, indicating that H_2 is more likely to remain in molecular form on these clusters.

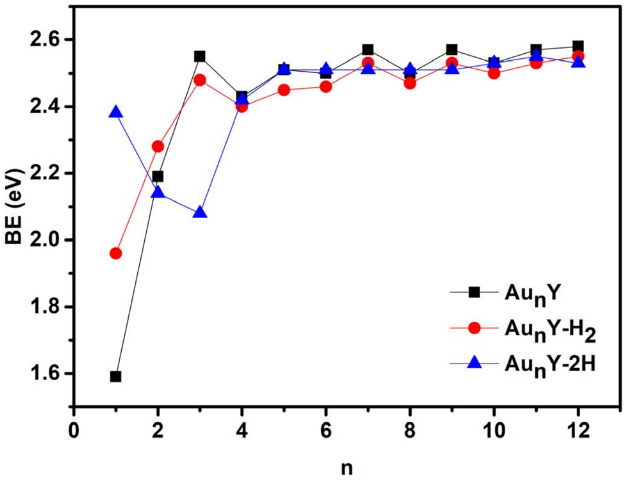

Fig. 2 Comparison of per-atom binding energies (BE, in eV) for Au_nY, $Au_nY–H_2$, and Au_nY–2H cluster.

5. Hydrogen adsorption process

The accumulation of small molecules on a surface is known as adsorption, which can be classified as either physisorption or chemisorption, depending on the nature of the interaction between the adsorbate and the surface. Physisorption is governed by weak van der Waals forces, whereas chemisorption involves the formation of chemical bonds. The adsorption process is influenced by several key factors, including the host cluster, the type of adsorption, and the energy barrier between the adsorbate and the surface. A comprehensive understanding of hydrogen adsorption on Au_nY (n = 2–12) clusters can be obtained through detailed analysis of bonding characteristics, particularly examining the interaction of a hydrogen molecule or two dissociated hydrogen atoms within a specific chemical equilibrium. To gain fundamental insights into the adsorption processes of H_2 on Au_nY clusters, we calculate the adsorption energy and H–H bond length for both molecular and dissociative adsorption configurations using the following equations:

$$E_{\mathrm{ads}}(\mathrm{Au}_n\mathrm{Y{-}H}_2) = E(\mathrm{Au}_n\mathrm{Y}) + E(\mathrm{H}_2) - E(\mathrm{Au}_n\mathrm{Y{-}H}_2) \tag{4}$$

Table 2 Comparison of calculated average biding energies per atom (BE/eV), adsorption energies (E_{ads}/eV), and H–H bond length (d_{H-H}/Å) for bare Au_nY clusters, molecular (H_2), and dissociative (2H) hydrogen adsorption on Au_nY (n = 1–12)

	BE/eV			E_{ads}/eV		d_{H-H}/Å	
n	Au_nY	$Au_nY–H_2$	Au_nY–2H	$Au_nY–H_2$	Au_nY–2H	$Au_nY–H_2$	Au_nY–2H
1	1.59	1.96	2.38	0.12	1.81	0.81	3.36
2	2.19	2.28	2.14	0.29	−0.39	0.85	4.16
3	2.55	2.48	2.08	0.15	−2.27	0.75	2.40
4	2.43	2.40	2.42	0.16	0.27	0.76	3.35
5	2.51	2.45	2.51	0.05	0.52	0.83	3.44
6	2.50	2.46	2.51	0.13	0.52	0.76	3.44
7	2.57	2.53	2.51	0.19	0.00	0.75	3.46
8	2.50	2.47	2.51	0.12	0.53	0.74	3.44
9	2.57	2.53	2.51	0.15	−0.11	0.76	3.45
10	2.53	2.50	2.53	0.14	0.56	0.74	3.46
11	2.57	2.53	2.55	0.13	0.40	0.74	3.51
12	2.58	2.55	2.53	0.27	−0.11	0.77	5.54

$$E_{\text{ads}}(\text{Au}_n\text{Y}-2\text{H}) = E(\text{Au}_n\text{Y}) + E(\text{H}_2) - E(\text{Au}_n\text{Y}-2\text{H}) \quad (5)$$

where $E(\text{Au}_n\text{Y})$, $E(\text{H}_2)$, $E(\text{Au}_n\text{Y}-\text{H}_2)$, and $E(\text{Au}_n\text{Y}-2\text{H})$ with $n = 2$–12 represent the optimized energies of bare Au_nY, isolated H_2, molecularly absorbed $\text{Au}_n\text{Y}–\text{H}_2$, and dissociatively absorbed $\text{Au}_n\text{Y}–2\text{H}$, respectively. The results are summarized in Table 2. A preliminary analysis reveals that, compared to the bond length of isolated H_2 (0.75 Å),[63] the H–H bond length ($d_{\text{H-H}}$) in $\text{Au}_n\text{Y}–\text{H}_2$ for $n = 1$–2, 4–6, 9, and 12 is significantly elongated, ranging from 0.76 to 0.85 Å. This increase in bond length indicates that H_2 undergoes activation upon adsorption on these Au_nY surfaces. In contrast, the distance between hydrogen atoms in $\text{Au}_n\text{Y}–2\text{H}$ clusters varies from 2.40 Å to 5.54 Å, confirming complete H_2 dissociation on the cluster surface.

The adsorption energies (E_{ads}) were calculated as the energy difference between the total energy of the reactants ($\text{Au}_n\text{Y} + \text{H}_2$) and the products ($\text{Au}_n\text{Y}–\text{H}_2$ or $\text{Au}_n\text{Y}–2\text{H}$), as expressed in eqn (4) and (5). In essence, E_{ads} represents the minimum energy required to desorb hydrogen from the clusters surface, as listed in Table 2. Comparing the adsorption energy of molecular and dissociative adsorption configurations, we find that all computed E_{ads} values for the molecular adsorption ($\text{Au}_n\text{Y}–\text{H}_2$) are positive, ranging from 0.05 to 0.29 eV, indicating that the formation of $\text{Au}_n\text{Y}–\text{H}_2$ is thermodynamically favorable. For dissociative adsorption ($\text{Au}_n\text{Y}–2\text{H}$), E_{ads} values range from −0.39 to 1.81 eV. Notably, the E_{ads} values for $\text{Au}_2\text{Y}–2\text{H}$, $\text{Au}_3\text{Y}–2\text{H}$, $\text{Au}_7\text{Y}–2\text{H}$, $\text{Au}_9\text{Y}–2\text{H}$, and $\text{Au}_{12}\text{Y}–2\text{H}$ clusters are negative or zero ($\text{Au}_7\text{Y}–2\text{H}$), suggesting that dissociative adsorption on

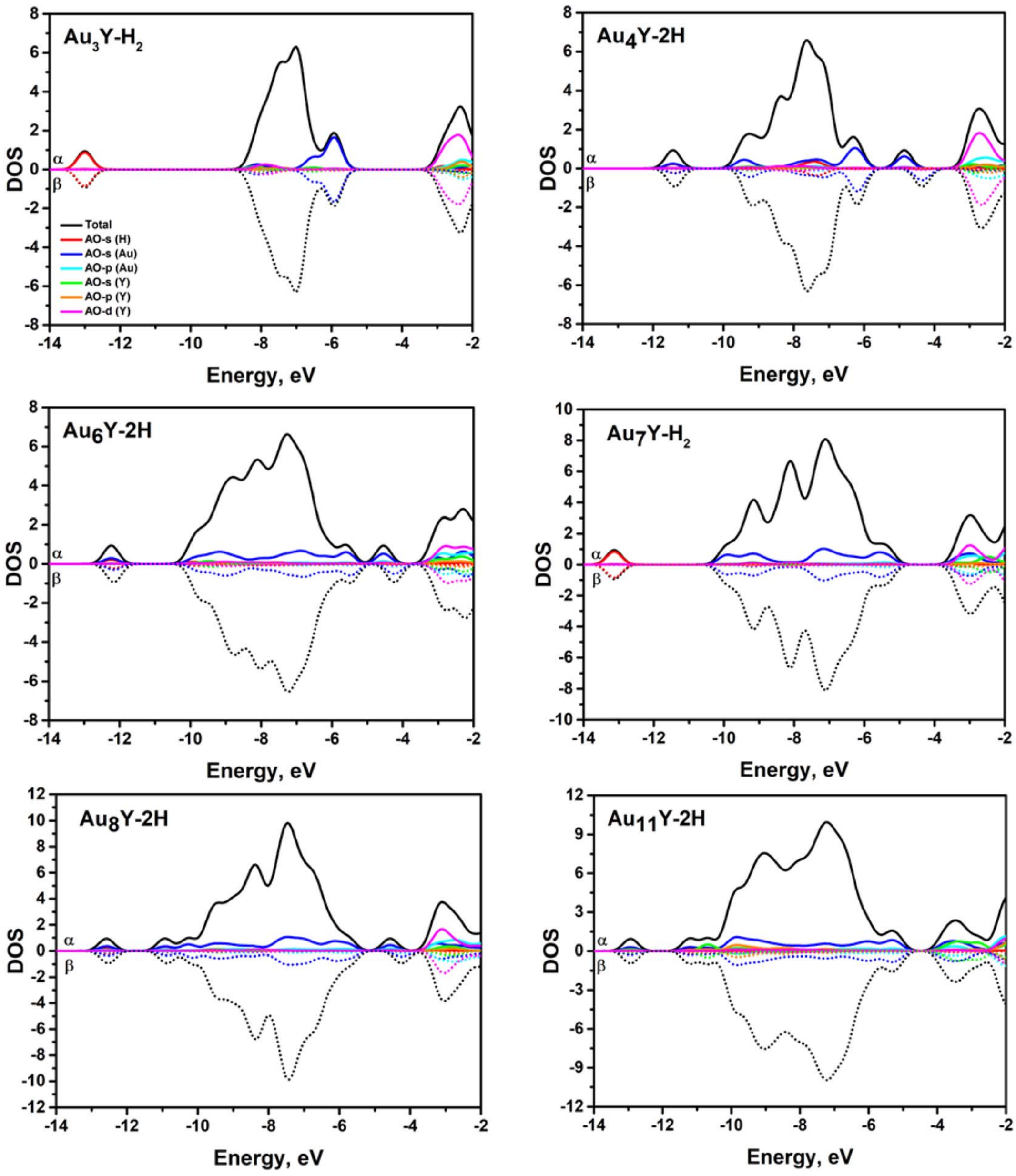

Fig. 3 Density of electronic states (DOS) for the most stable configuration of hydorgen adsorbed on Au_nY ($n = 3$–4, 6–8, and 11) clusters.

these clusters is endothermic and unlikely to occur spontaneously. This phenomenon can be attributed to the decrease in average binding energy for these clusters compared to their bare counterparts (Au_2Y, Au_3Y, Au_7Y, Au_9Y, and $Au_{12}Y$). In contrast, H_2 dissociation on Au_nY–2H ($n = 1$, 4–6, 8, 10 and 11) clusters is exothermic and thermodynamically favorable, as evidenced by the higher computed E_{ads} values for dissociative adsorption Au_nY–2H compared to molecular adsorption Au_nY–H_2. It is worth mentioning that molecular adsorption is more likely to occur for Au_nY with $n = 2$, 3, 7, 9, and 12. On the other hand, when H_2 approaches the surface of Au_nY ($n = 1$, 4–6, 8, 10, and 11), it first undergoes molecular adsorption. Subsequently, the hydrogen molecule may either desorb from the cluster surface or eventually undergo dissociation, forming strong atomic bonds with the cluster. The detachment of adsorbed H_2 molecules may dominate in certain cases, as it is influenced not only by adsorption energy but also by the activation barrier of the transition state and multiple intermediate states before reaching a stable dissociative configuration. A more detailed discussion on this topic will be provided in the following sections.

To better understand the binding nature of adsorbed hydrogen molecules on Au_nY ($n = 1$–12) clusters, we analyzed the densities of electronic states (DOS) for both molecular and dissociative adsorption configurations. The DOS results for several thermodynamically preferred configurations are illustrated in Fig. 3, while data for other species are provided in the ESI.† [46] For each DOS graph in Fig. 3, both partial and total DOS are depicted. Solid lines represent spin-up (α) states, whereas dashed lines correspond to spin-down (β) states. As shown in Fig. 3, for species where physisorption is energetically feasible (Au_nY–H_2 with $n = 3$, 7), most of electronic states associated with adsorbed hydrogen (red line) appear on the low-energy side (below −13.0 eV), indicating a weak interaction between hydrogen and the cluster surface. These states are clearly separated from the electronic states of the cluster, which extend beyond −8.5 eV for $n = 3$ and −10.5 eV for $n = 7$, respectively. This indicates that the chemical bonding contribution between hydrogen and these clusters is relatively weak or potentially negligible. This observation aligns well with previous studies on molecular hydrogen adsorption in transition metal-doped Ag_n ($n = 2$–12), Au_{10}^{2+} or even $[Mo_{13}S_{13}]^{2-}$ clusters, where van der Waals forces and/or electrostatic interactions between charge-polarized hydrogen molecules and cluster surfaces were identified as the dominant bonding mechanisms.[42,43,67]

The DOS for dissociative configurations of Au_nY–2H ($n = 4$, 6, 8, 11) in Fig. 3, along with additional results for $n = 1$, 5, and 10 provided in the ESI,† [46] exhibit a distinctly different behavior compared to their molecular adsorption counterparts. Remarkably, an analysis of the DOS spectra reveals an intriguing observation: the expected low-energy contribution of s-H_2 states, typically associated with molecular adsorption, disappears entirely in the dissociative configurations. Instead, the electronic states of hydrogen extend significantly toward higher energies, generally exceeding −10.5 eV, with the exception of $n = 1$ and 4, where they remain above −8.5 eV. This shift is attributed to the strong hybridization of valence s-electrons from hydrogen atoms with those of the cluster, leading to the formation of stable chemical bonds within these systems. Additionally, in most cases, the highest occupied molecular orbital (HOMO) states are predominantly contributed by s-Au orbitals, further reinforcing the role of gold in hydrogen dissociation mechanisms. It is important to note that bonding interactions are often accompanied by electron transfer processes. Therefore, these findings support the earlier conclusion that hydrogen adsorption preferentially occurs at Au surface sites.

To gain deeper insight into the dissociative hydrogen adsorption mechanism in Au_nY–2H ($n = 1$, 4–6, 8, 10 and 11) clusters, we computed possible reaction pathways linking the reactants to their final dissociated states for single H_2 adsorption and dissociation. Fig. 4 presents the hydrogen dissociation pathways for Au_4Y, Au_6Y, Au_8Y, and $Au_{11}Y$ clusters, while additional data for AuY, Au_5Y, and $Au_{10}Y$ are provided in the ESI.† [46] The activation energy for hydrogen dissociation was determined by incorporating zero-point energy corrections and electronic energy values of the reactants and transition states (TS). Specifically, the activation barrier is quantified as the total energy difference between the reactants and the TS, offering insights into the feasibility of hydrogen dissociation on Au_nY clusters.

As shown in Fig. 4, the interaction of H_2 with Au_4Y clusters follows a stepwise dissociative adsorption mechanism. Initially, molecular hydrogen preferentially binds to the transition metal atom Y with an adsorption energy of −0.16 eV. However, to activate the adsorbed H_2, the Au_4Y clusters must overcome two activation barriers (TS_1 and TS_2) associated with the dissociation process. The first activation barrier is 0.78 eV (+0.62 eV relative to the reactants at −0.16 eV), while the second barrier is 0.73 eV (+0.60 eV relative to the intermediate state I_1 at −0.13 eV). Before reaching the final dissociated product (Au_4Y–2H), the system passes through another intermediate state (I_2) at 0.44 eV. The final state, where the H_2 molecule is fully dissociated, has an energy of −0.27 eV, which is 0.11 eV lower than the reactant state (−0.16 eV), indicating a thermodynamically favorable process. A similar dissociative adsorption mechanism is observed for Au_nY clusters with $n = 1$, 5, 6, 8, 10 and 11). As detailed in the ESI,† the Au_5Y cluster follows a comparable pathway. The activation barrier for H_2 dissociation (TS_1) is 0.75 eV (+0.70 eV relative to the reactant state), followed by a significant energy decrease through the intermediate state I_1 (−0.04 eV). Ultimately, the system reaches a fully dissociated state, forming Au_5Y–2H with an energy of −0.52 eV, which is 0.47 eV lower than both the reactants and the H_2 adsorption state (−0.05 eV).

Similarly, for Au_6Y cluster, H_2 activation requires overcoming an energy barrier of 0.68 eV for the first transition state (TS_1, +0.55 eV relative to the reactant state). The system then proceeds through an intermediate state (I_1) with a slight energy drop of 0.21 eV before reaching the final dissociated state, which is 0.39 eV lower than the initial molecular adsorption state (−0.13 eV). A similar dissociative adsorption pattern is observed for AuY, Au_8Y and $Au_{10}Y$ clusters. The activation barriers for the first transition state are 0.48 eV, 0.74 eV and

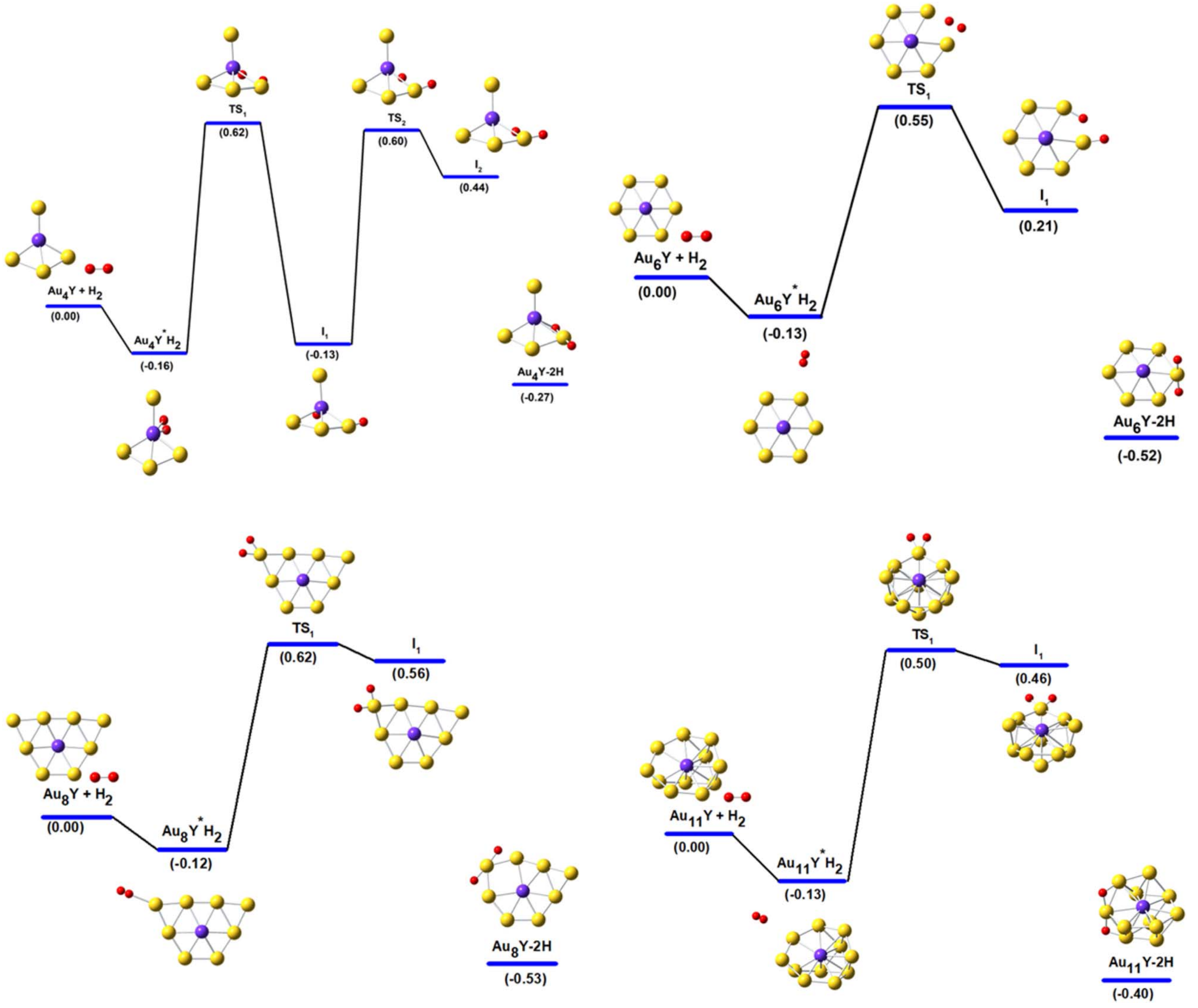

Fig. 4 Computed reaction pathways and relative energies (in eV) for H_2 dissociative adsorption on Au_4Y, Au_6Y, Au_8Y, and $Au_{11}Y$ clusters. Intermediates and transition states are denoted as I_i and TS_i, respectively. Yellow, purple, and red spheres represent Au, Y, and H atoms, respectively.

0.80 eV for the transition state TS_1 (0.36 eV, 0.62 eV and 0.66 eV relative to the reactant state), respectively. Before reaching their final stable states, Au_8Y and $Au_{10}Y$ pass through intermediate states with energy drops of +0.56 eV and −0.28 eV, respectively. In contrast, the AuY cluster reaches its final state at −1.81 eV without any intermediate states. Interestingly, the $Au_{11}Y$ cluster exhibits the lowest activation energy for H_2 dissociation among the studied clusters, with a barrier of 0.63 eV for TS_1 (+0.50 eV). The system transitions through an intermediate state (I_1, +0.46 eV) before fully dissociating into the most stable state, $Au_{11}Y$–2H, at −0.40 eV (0.27 eV lower than the reactants and the H_2 adsorption state, −0.13 eV). Comparing the activation barriers for H_2 dissociation across Au_5Y (0.75 eV), Au_6Y (0.68 eV), Au_8Y (0.74 eV), $Au_{10}Y$ (0.80 eV), and $Au_{11}Y$ (0.63 eV), it is evident that the $Au_{10}Y$ cluster exhibits the highest energy barrier at 0.8 eV, suggesting a more challenging dissociative adsorption process compared to other clusters.

Although the final products of H_2 dissociation on the Au_4Y, Au_5Y, Au_8Y, and $Au_{10}Y$ clusters exhibit relatively low energies of −0.27 eV, −0.52 eV, −0.53 eV, and −0.56 eV, respectively, the activation energy barriers for H_2 dissociation remain relatively high at 0.78 eV, 0.75 eV, 0.74 eV, and 0.80 eV. This suggests that while H_2 adsorption is energetically favorable for these clusters, dissociative adsorption is unlikely to occur without external stimuli, particularly for the Au_4Y and $Au_{10}Y$ clusters. For the AuY cluster, the activation barrier for adsorption-dissociation is relatively low at 0.48 eV, and the final product has a significantly low energy of −1.81 eV. However, as previously mentioned, this cluster is known to be unstable, limiting its potential for real-world catalytic applications. In contrast, the Au_6Y and $Au_{11}Y$ clusters exhibit the lowest activation energy barriers of 0.68 eV and 0.63 eV, respectively. This indicates that Au_6Y and $Au_{11}Y$ could serve as promising superatoms for hydrogen storage applications.

6. Conclusion

In summary, we have systematically investigated the interaction of H_2 with small-sized Au_nY clusters ($n = 1$–12) using DFT calculations. Our findings highlight the crucial role of transition metal dopants in stabilizing cluster geometries and enhancing reactivity toward hydrogen adsorption and dissociation. We identified that the geometric structure, relative electronegativity of the dopant atom, and atomic coordination number (N) are key factors governing the preferred adsorption configurations. The Y atom exhibits a strong preference for high-coordination sites, favoring surface positions in smaller clusters ($n = 1$–5) before becoming gradually encapsulated by Au atoms in larger clusters ($n = 6$–12). Due to its relatively lower electronegativity ($\chi_Y = 1.22$) compared to gold ($\chi_{Au} = 2.54$), H_2 adsorption initially favors direct interaction with Y. However, as cluster size increases ($n = 7$–12) and the Y dopant attains higher coordination numbers, hydrogen adsorption shifts toward Au surface sites or Au–Au bridge positions. Notably, our results also indicate that molecular hydrogen adsorption does not significantly alter the structure of bare Au_nY clusters (except for Au_5Y). The adsorption of two dissociated hydrogen atoms preferentially occurs at Au–Au or Au–Y bridge sites, depending on cluster size and atomic arrangement. Average binding energy calculations reveal that the hydrogen adsorption on Au_nY ($n = 4$–12) generally maintains higher relative stability compared to their bare counterparts. Importantly, dissociative adsorption is unlikely to occur for Au_nY ($n = 1$, 4–5, 8, 10) clusters without external stimulation due to high energy barriers, while for $n = 2$, 3, 7, and 9 molecular adsorption is energetically preferred. Au_6Y and $Au_{11}Y$ clusters exhibit remarkable stability and barrier-free dissociation pathways, making them promising candidates for hydrogen dissociation and storage applications. Our results provide a deeper insight into the interaction between H_2 and Au_nY clusters, including the adsorption site preference, the stability of adsorption configuration, the effect of impurities, possible reaction pathways, and energy barriers involved with this process. This work offers valuable guidance for future experiments and contributes to the development of alloys metal clusters as fundamental components in the design of innovative nanostructured materials for hydrogen catalysis and storage applications.

Data availability

The data supporting this article have been included as part of the ESI.†

Author contributions

Nguyen Van Dang: conceptualization, data curation, formal analysis, investigation, validation, writing – original draft, review and editing. Ngo Thi Lan: conceptualization, funding acquisition, data curation, validation, writing – original draft, review and editing. Nguyen Thi Mai: data curation, formal analysis, investigation, validation, review and editing. Son Tung Ngo: data curation, formal analysis, investigation, validation, review and editing. Phung Thi Thu: data curation, formal analysis, investigation, validation. Nguyen Thanh Tung: conceptualization, data curation, formal analysis, investigation, validation, writing – original draft, review and editing.

Conflicts of interest

There are no conflicts to declare.

Acknowledgements

This research was financially supported by the National Foundation of Science and Technology Development (NAFOSTED) under the grant number 103.01-2021.109.

Notes and references

1 L. Schlapbach and A. Züttel, Hydrogen-storage materials for mobile applications, *Nature*, 2001, **414**(6861), 353–358.
2 L. Baetcke and M. Kaltschmitt, *Hydrogen Storage for Mobile Application: Technologies and Their Assessment, Hydrogen Supply Chains*, Elsevier, 2018, pp. 167–206.
3 A. Pareek, R. Dom, J. Gupta, J. Chandran, V. Adepu and P. H. Borse, Insights into renewable hydrogen energy: recent advances and prospects, *Mater. Sci. Energy Technol.*, 2020, **3**, 319–327.
4 G. Nicoletti, N. Arcuri, G. Nicoletti and R. Bruno, A technical and environmental comparison between hydrogen and some fossil fuels, *Energy Convers. Manage.*, 2015, **89**, 205–213.
5 M. Yue, H. Lambert, E. Pahon, R. Roche, S. Jemei and D. Hissel, Hydrogen energy systems: a critical review of technologies, applications, trends and challenges, *Renew. Sustainable Energy Rev.*, 2021, **146**, 111180.
6 N. Klopčič, I. Grimmer, F. Winkler, M. Sartory and A. Trattner, A review on metal hydride materials for hydrogen storage, *J. Energy Storage*, 2023, **72**, 108456.
7 C. Drawer, J. Lange and M. Kaltschmitt, Metal hydrides for hydrogen storage–Identification and evaluation of stationary and transportation applications, *J. Energy Storage*, 2024, **77**, 109988.
8 F. J. Desai, M. N. Uddin, M. M. Rahman and R. Asmatulu, A critical review on improving hydrogen storage properties of metal hydride *via* nanostructuring and integrating carbonaceous materials, *Int. J. Hydrogen Energy*, 2023, **48**(75), 29256–29294.
9 I. Hassan, H. S. Ramadan, M. A. Saleh and D. Hissel, Hydrogen storage technologies for stationary and mobile applications: review, analysis and perspectives, *Renew. Sustainable Energy Rev.*, 2021, **149**, 111311.
10 F. Schüth, Challenges in hydrogen storage, *Eur. Phys. J. Special Top.*, 2009, **176**, 155–166.
11 W. L. L. Sun, Z. Li, M. Fujii, Y. Geng, L. Dong and T. Fujita, Trends and future challenges in hydrogen production and storage research, *Environ. Sci. Pollut. Res.*, 2020, **27**, 31092–31104.
12 P. H. M. Babaie, F. Salek, N. Haque, R. Savage, S. Stevanovic, T. A. Bodisco and A. Zare, Advancements in hydrogen

production, storage, distribution and refuelling for a sustainable transport sector: hydrogen fuel cell vehicles, *Int. J. Hydrogen Energy*, 2024, **52**, 973–1004.

13 P. Nordlander, S. Holloway and J. Nørskov, Hydrogen adsorption on metal surfaces, *Surf. Sci.*, 1984, **136**(1), 59–81.

14 B. Kumar, T. Kawawaki, N. Shimizu, Y. Imai, D. Suzuki, S. Hossain, L. V. Nair and Y. Negishi, Gold nanoclusters as electrocatalysts: size, ligands, heteroatom doping, and charge dependences, *Nanoscale*, 2020, **12**(18), 9969–9979.

15 Y. Gao, N. Shao, Y. Pei, Z. Chen and X. C. Zeng, Catalytic activities of subnanometer gold clusters (Au_{16}–Au_{18}, Au_{20}, and Au27–Au_{35}) for CO oxidation, *ACS Nano*, 2011, **5**(10), 7818–7829.

16 M. S. Bootharaju, C. W. Lee, G. Deng, H. Kim, K. Lee, S. Lee, H. Chang, S. Lee, Y. E. Sung, J. S. Yoo, N. Zheng and T. Hyeon, Atom-precise heteroatom core-tailoring of nanoclusters for enhanced solar hydrogen generation, *Adv. Mater.*, 2023, **35**(18), 2207765.

17 L. M. Wang, S. Bulusu, W. Huang, R. Pal, L.-S. Wang and X. C. Zeng, Doping the golden cage Au_{16}^{-} with Si, Ge, and Sn, *J. Am. Chem. Soc.*, 2007, **129**(49), 15136–15137.

18 R. Pal, L.-M. Wang, W. Huang, L.-S. Wang and X. C. Zeng, Structural evolution of doped gold clusters: MAu_x^{-}($M = Si$, Ge, Sn; $x = 5- 8$), *J. Am. Chem. Soc.*, 2009, **131**(9), 3396–3404.

19 L. M. Wang, S. Bulusu, H. J. Zhai, X. C. Zeng and L. S. Wang, Doping golden buckyballs: $Cu@Au_{16}^{-}$ and $Cu@Au_{17}^{-}$ cluster anions, *Angew. Chem., Int. Ed.*, 2007, **46**(16), 2915–2918.

20 R. Pal, L.-M. Wang, Y. Pei, L.-S. Wang and X. C. Zeng, Unraveling the mechanisms of O_2 activation by size-selected gold clusters: transition from superoxo to peroxo chemisorption, *J. Am. Chem. Soc.*, 2012, **134**(22), 9438–9445.

21 M. A. Dar and S. Krishnamurty, Molecular and dissociative adsorption of oxygen on Au–Pd bimetallic clusters: role of composition and spin state of the cluster, *ACS Omega*, 2019, **4**(7), 12687–12695.

22 D. Manzoor, S. Krishnamurty and S. Pal, Effect of silicon doping on the reactivity and catalytic activity of gold clusters, *J. Phys. Chem. C*, 2014, **118**(14), 7501–7507.

23 D. Manzoor, S. Krishnamurty and S. Pal, Endohedrally doped gold nanocages: efficient catalysts for O_2 activation and CO oxidation, *Phys. Chem. Chem. Phys.*, 2016, **18**(10), 7068–7074.

24 D. Manzoor, S. Krishnamurty and S. Pal, Contriving a catalytically active structure from an inert conformation: a density functional investigation of Al, Hf, and Ge doping of Au_{20} tetrahedral clusters, *J. Phys. Chem. C*, 2016, **120**(35), 19636–19641.

25 L. Li, Y. Gao, H. Li, Y. Zhao, Y. Pei, Z. Chen and Z. C. Zeng, CO oxidation on TiO_2 (110) supported subnanometer gold clusters: size and shape effects, *J. Am. Chem. Soc.*, 2013, **135**(51), 19336–19346.

26 S. Maity, S. Takano, S. Masuda and T. Tsukuda, Bonding and electronic interactions of hydrogen with gold superatoms, *J. Phys. Chem. C*, 2023, **128**(1), 19–30.

27 D. Manzoor and S. Pal, Hydrogen atom chemisorbed gold clusters as highly active catalysts for oxygen activation and CO oxidation, *J. Phys. Chem. C*, 2014, **118**(51), 30057–30062.

28 K. Mondal, S. Agrawal, D. Manna, A. Banerjee and T. K. Ghanty, Effect of hydrogen atom doping on the structure and electronic properties of 20-atom gold cluster, *J. Phys. Chem. C*, 2016, **120**(33), 18588–18594.

29 Megha, C. Kamal, K. Mondal, T. K. Ghanty and A. Banerjee, Remarkable structural effect on the gold–hydrogen analogy in hydrogen-doped gold cluster, *J. Phys. Chem. A*, 2019, **123**(10), 1973–1982.

30 S. Buckart, G. Ganteför, Y. D. Kim and P. Jena, Anomalous behavior of atomic hydrogen interacting with gold clusters, *J. Am. Chem. Soc.*, 2003, **125**(46), 14205–14209.

31 X. Ma, S. Liu and S. Huang, Hydrogen adsorption and dissociation on the TM-doped (TM= Ti, Nb) Mg_{55} nanoclusters: A DFT study, *Int. J. Hydrogen Energy*, 2017, **42**(39), 24797–24810.

32 D. Shen, C.-P. Kong, R. Jia, P. Fu and H.-X. Zhang, Investigation of properties of Mg n clusters and their hydrogen storage mechanism: a study based on DFT and a global minimum optimization method, *J. Phys. Chem. A*, 2015, **119**(15), 3636–3643.

33 D. Shi, Y. Ni, G. Li, Z. Yan, Q. Zhao, W. Zhao, W. Xie, X. Meng and J. Chen, A computational study of Mg_mH_n nanoclusters with $n: m \geq 2:1$ for efficient hydrogen storage, *Int. J. Quantum Chem.*, 2023, **123**(6), e27058.

34 M. Pozzo and D. Alfe, Hydrogen dissociation and diffusion on transition metal (=Ti, Zr, V, Fe, Ru, Co, Rh, Ni, Pd, Cu, Ag)-doped Mg (0001) surfaces, *Int. J. Hydrogen Energy*, 2009, **34**(4), 1922–1930.

35 J. Li, Y. Liu, J. Zhang, X. Liang and H. Duan, Density functional theory study of the adsorption of hydrogen atoms on Cu_2X ($X = 3d$) clusters, *Chem. Phys. Lett.*, 2016, **651**, 137–143.

36 W. C. G. Hu, K. Kwak, M. Kim, D. Jiang, J. Choi and D. Lee, Effects of metal-doping on hydrogen evolution reaction catalyzed by MAu_{24} and M_2Au_{36} nanoclusters ($M = Pt$, Pd), *ACS Appl. Mater. Interfaces*, 2018, **10**(51), 44645–44653.

37 Z. Fang and X. Kuang, Hydrogen molecule adsorption on Au_nPt ($n = 1$–12) clusters in comparison with corresponding pure Au_{n+1} ($n = 1$–12) clusters, *Phys. Status Solidi B*, 2014, **251**(2), 446–454.

38 Y. Li, Y.-F. Li, J.-J. Tan, B.-F. Jiang and Y.-Z. OuYang, Probing structure, electronic property, and hydrogen adsorption for the alkali auride series, *Eur. Phys. J. Plus*, 2017, **132**(4), 159.

39 D. Bandyopadhyay, S. Chatterjee, R. Trivedi and K. Dhaka, Insights into catalytic behavior of $TiMg_n$ ($n = 1$–12) nanoclusters in hydrogen storage and dissociation process: a DFT investigation, *Int. J. Hydrogen Energy*, 2022, **47**(27), 13418–13429.

40 J. Vanbuel, M. Jia, P. Ferrari, S. Gewinner, W. Schöllkopf, M. T. Nguyen, A. Fielicke and E. Janssens, Competitive molecular and dissociative hydrogen chemisorption on size selected doubly rhodium doped aluminum clusters, *Top. Catal.*, 2018, **61**, 62–70.

41 M. Jia, J. Vanbuel, P. Ferrari, E. M. Fernández, S. Gewinner, W. Schöllkopf, M. T. Nguyen, A. Fielicke and E. Jansses, Size dependent H_2 adsorption on Al_nRh^+ (n = 1–12) clusters, *J. Phys. Chem. C*, 2018, **122**(32), 18247–18255.

42 N. T. Lan, N. T. Mai, N. T. Cuong, P. T. H. Van, D. D. La, N. M. Tam, S. T. Ngo and N. T. Tung, Exploring hydrogen adsorption on nanocluster systems: insights from DFT calculations of Au_9M^{2+} (M = Sc-Ni), *Chem. Phys. Lett.*, 2023, **831**, 140838.

43 N. T. Lan, N. T. Mai, N. T. Cuong, P. T. H. Van, D. D. La, N. M. Tam, S. T. Ngo and N. T. Tung, Density functional study of size-dependent hydrogen adsorption on Ag_nCr (n = 1–12) clusters, *ACS Omega*, 2022, **7**(42), 37379–37387.

44 A. S. Shajahan, N. Kalarikkal, N. Garg, Y. Kawazo and B. Chakraborty, A quest to high-capacity hydrogen storage in zirconium decorated pentagraphene: DFT perspectives, *Int. J. Hydrogen Energy*, 2022, **47**(85), 36190–36203.

45 C. Guo and C. Wang, The hydrogen storage capacities of 4d transition metals in various boron systems, *J. Energy Storage*, 2023, **57**, 106216.

46 M. D. Esrafili and S. Sadeghi, Y decorated all-boron B_{38} nanocluster for reversible molecular hydrogen storage: a first-principles investigation, *Int. J. Hydrogen Energy*, 2022, **47**(22), 11611–11621.

47 W. Liu, Y. Liu and R. Wang, Prediction of hydrogen storage on Y-decorated graphene: a density functional theory study, *Appl. Surf. Sci.*, 2014, **296**, 204–208.

48 M. El, K. M. Bhihi, S. Naji, H. Labrim, A. Benyoussef, A. El Kenz and M. Loulidi, Study of doping effects with 3d and 4d-transition metals on the hydrogen storage properties of MgH_2, *Int. J. Hydrogen Energy*, 2016, **41**(8), 4712–4718.

49 J. Lyu, V. Kudiiarov, L. Svyatkin, A. Lider and K. Dai, On the catalytic mechanism of 3d and 4d transition-metal-based materials on the hydrogen sorption properties of Mg/MgH_2, *Catalysts*, 2023, **13**(3), 519.

50 C. Sergio, F. Pansini and M. de Campos, The relationship between hydrogen storage capacity and 4d transition metal–carbon surface binding energy, *Chem. Phys. Lett.*, 2024, **846**, 141338.

51 J. Barabás, P. Ferrari, V. Kaydashev, J. Vanbuel, E. Janssens and T. Höltzl, The effect of size, charge state and composition on the binding of propene to yttrium-doped gold clusters, *RSC Adv.*, 2021, **11**(47), 29186–29195.

52 Q. L. M. Paskevicius, D. A. Sheppard, C. E. Buckley and A. W. Thornton, Hydrogen storage materials for mobile and stationary applications: current state of the art, *ChemSusChem*, 2015, **8**(17), 2789–2825.

53 M. L. S. Srivastava, T. Lakshmi, E. R. Sandadi, S. Gour, N. A. Thomas, S. S. Priya and K. Sudhakar, An overview of hydrogen storage technologies–Key challenges and opportunities, *Mater. Chem. Phys.*, 2024, **325**, 129710.

54 M. D. Liptak and G. C. Shields, Comparison of density functional theory predictions of gas-phase deprotonation data, *Int. J. Quantum Chem.*, 2005, **105**(6), 580–587.

55 M. Frisch G. W. Trucks, H. B. Schlegel, M. J. Frisch, G. W. Trucks, H. B. Schlegel, G. E. Scuseria, M. A. Robb, J. R. Cheeseman, G. Scalmani, V. Barone, B. Mennucci and G. A. Petersson, *Gaussian 09, Revision a. 02, 200*, Gaussian, Inc., Wallingford, CT, 2009, p. 271.

56 P. Hohenberg and W. Kohn, Inhomogeneous electron gas, *Phys. Rev.*, 1964, **136**(3B), B864.

57 T. B. Tai and M. T. Nguyen, A stochastic search for the structures of small germanium clusters and their anions: enhanced stability by spherical aromaticity of the Ge_{10} and $Ge_{12}{}^{2-}$ systems, *J. Chem. Theory Comput.*, 2011, **7**(4), 1119–1130.

58 Q. Du, X. Wu, P. Wang, D. Wu, L. Sai, R. B. King, S. J. Park and J. Zhao, Structure evolution of transition metal-doped gold clusters M@Au_{12} (M= 3d–5d): Across the periodic table, *J. Phys. Chem. C*, 2020, **124**(13), 7449–7457.

59 R. McWeeny and B. T. Sutcliffe, Fundamentals of self-consistent-field (SCF), hartree-fock (HF), multi-configuration (MC) SCF and configuration interaction (CI) schemes, *Comput. Phys. Rep.*, 1985, **2**(5), 219–278.

60 F. Weinhold, *Discovering Chemistry with Natural Bond Orbitals*, John Wiley & Sons, 2012.

61 C. Peng, P. Y. Ayala, H. B. Schlegel and M. J. Frisch, Using redundant internal coordinates to optimize equilibrium geometries and transition states, *J. Comput. Chem.*, 1996, **17**(1), 49–56.

62 N. Govind, M. Petersen, G. Fitzgerald, D. King-Smith and J. Andzelm, A generalized synchronous transit method for transition state location, *Comput. Mater. Sci.*, 2003, **28**(2), 250–258.

63 Y.-R. Luo, *Comprehensive Handbook of Chemical Bond Energies*, CRC press, 2007.

64 L. Rincon, A. Hasmy, M. Marquez and C. Gonzalez, A perturbatively corrected tight-binding method with hybridization: application to gold nanoparticles, *Chem. Phys. Lett.*, 2011, **503**(1–3), 171–175.

65 L. Lin, P. Claes, P. Gruene, G. Mijer, A. Fielicke, M. T. Nguyen and P. Lievens, Far-infrared spectra of yttrium-doped gold clusters Au_nY (n = 1–9), *Chem. Phys. Chem.*, 2010, **11**(9), 1932–1943.

66 L. Guo, First-principles study of molecular hydrogen adsorption and dissociation on Al_nCr (n = 1–13) clusters, *J. Phys. Chem. A*, 2013, **117**(16), 3458–3466.

67 T. T. Phung, N. T. Huyen, N. T. Giang, N. M. Thu, N. T. Son, N. H. Tung, N. T. Lan, N. T. Mai and N. T. Tung, Unraveling hydrogen adsorption on transition metal-doped $[Mo_3S_{13}]^{2-}$ clusters: insights from density functional theory calculations, *ACS Omega*, 2024, **19**, 18.

68 J. K. J. Greeley, N. A. Romero, V. A. Morozov, H. Falsig, A. H. Larsen, J. Lu, J. J. Mortensen, M. Dułak, K. S. Thygesen, J. K. Nørskov and K. W. Jacobse, Finite size effects in chemical bonding: from small clusters to solids, *Catal. Lett.*, 2011, **141**, 1067–1071.

69 R. Trivedi and D. Bandyopadhyay, Hydrogen storage in small size MgnCo clusters: a density functional study, *Int. J. Hydrogen Energy*, 2015, **40**(37), 12727–12735.

70 G. Ortega, E. Germán, M. J. Lopez and J. A. Alonso, Catalytic activity of Co–Ag nanoalloys to dissociate molecular hydrogen. New insights on the chemical environment, *Int. J. Hydrogen Energy*, 2022, **47**(44), 19038–19050.